

Ordering leads to multiple fast tracks in simulated collective escape of human crowds

Chen Cheng,^a Jinglai Li,^b and Zhenwei Yao^{c*}

^a *School of Mathematical Sciences, Shanghai Jiao Tong University, Shanghai 200240, China*

^b *School of Mathematics, University of Birmingham, Edgbaston, Birmingham B15 2TT, UK*

^c *School of Physics and Astronomy, and Institute of Natural Sciences, Shanghai Jiao Tong University, Shanghai 200240, China*

Elucidating emergent regularities in intriguing crowd dynamics is a fundamental scientific problem arising in multiple fields. In this work, based on the social force model, we simulate the typical scenario of collective escape towards a single exit and reveal the striking analogy of crowd dynamics and crystallisation. With the outflow of the pedestrians, crystalline order emerges in the compact crowd. In this process, the local misalignment and global rearrangement of pedestrians are well rationalized in terms of the characteristic motions of topological defects in the crystal. Exploiting the notions from the physics of crystallisation further reveals the emergence of multiple fast tracks in the collective escape.

I. INTRODUCTION

Collective motion of pedestrians is a common phenomenon in various daily scenarios of urban life, and once driven by life-threatening panic, overcrowding and stampede may lead to fatalities [1–10]. Understanding crowd dynamics is thus crucial for achieving safety and efficiency at both individual and collective levels [11–14]. Observations show that the majority of pedestrians walk in groups [15], and the size of free-forming groups conforms to Poisson distribution, indicating the existence of statistical regularity in complicated crowd behaviours [16–18]. Collective phenomena, such as oscillational behaviour [19] and the fast-is-slower [20, 21] and stop-and-go [22–24] effects, are experimentally observed [12, 25]. Quantitative measurement of pedestrian flows further reveals an analogy with the Navier-Stokes equations that originally describe dynamics of fluids [26, 27]. The phenomenological fluid-dynamic approach captures macroscopic behaviours of crowd dynamics by averaging the behaviours of neighbouring individuals [28, 29].

Further scrutiny of individual pedestrians could provide valuable microscopic information that yields insights into the intriguing crowd dynamics [12, 18, 30–34]. Following this idea, a social force model (SFM) has been proposed to simulate the motion of human crowds [1, 12, 35]. The basic idea underlying the SFM is to treat pedestrians as particles with a simplified will. Specifically, this model features a mixture of both physical and socio-psychological forces influencing the walking behaviour of pedestrians, and it has the unique advantage of incorporating new forces as our understanding of pedestrians is advanced [1, 12, 15]. Much has been learned about the law of crowd dynamics by applying the SFM in various situations [3, 12, 15, 36].

While the SFM could conveniently provide detailed dynamical information of crowd motion by specifying

proper values of model parameters [12], the challenge is to exploit the simulated data from a suitable perspective for revealing the underlying regularities. In this work, we resort to the analogy of crowd dynamics and crystallisation process [37–39], and gain insights into the intriguing collective motion. Specifically, we simulate the typical scenario of collective escape towards a single exit using the generalized social force model that incorporates the random behaviours of pedestrians. Our simulations show the rapid ordering of the initially randomly distributed pedestrians. In the compact “crystallised” crowd, local misalignments emerge at random sites, which are recognised as topological defects in two-dimensional crystal [37, 40]. With the outflow of pedestrians, the microscopic crystalline structure underlying the crowd is under persistent transformation, which exactly corresponds to the characteristic annihilation and glide motion of topological defects in the crystal. From the striking analogy between crowd dynamics and crystallisation process, and in combination with statistical analysis, we demonstrate the emergence of multiple fast tracks resulting from the spontaneously formed crystal structure in the escaping crowd. This work reveals the regularities in crowd dynamics from the perspective of crystallisation, and may provide useful information for understanding crowd behaviours in evacuation.

II. MODEL AND METHOD

We simulate the crowd dynamics of pedestrians based on the SFM [12]. It assumes a mixture of physical and socio-psychological forces influencing the crowd behaviour by considering personal motivations and environmental constraints. In this model, each pedestrian i of mass m_i and velocity \mathbf{v}_i tends to move by a desired speed v_i^p along a certain direction \mathbf{e}_i^p during the acceleration time τ_i . The resulting personal desire force \mathbf{F}_p is:

$$\mathbf{F}_p = m_i \frac{v_i^p \mathbf{e}_i^p - \mathbf{v}_i}{\tau_i}. \quad (1)$$

*Electronic address: zyao@sjtu.edu.cn

Here, we note that the pedestrians are polarised to proceed towards the exit, since the desired direction of motion always points to the exit in the model. Furthermore, pedestrians psychologically tend to keep a social distance between each other and avoid hitting walls. This is modelled by introducing “interaction force” \mathbf{f}_{ij} between pedestrians i and j and \mathbf{f}_{iW} between pedestrian i and the wall, respectively. The total interaction force is

$$\mathbf{F}_{int} = \sum_{j(\neq i)} \mathbf{f}_{ij} + \sum_W \mathbf{f}_{iW}. \quad (2)$$

Combining eqn (1) and (2), we obtain the acceleration equation

$$m_i \frac{d\mathbf{v}_i}{dt} = m_i \frac{v_i^p(t) \mathbf{e}_i^p(t) - \mathbf{v}_i(t)}{\tau_i} + \sum_{j(\neq i)} \mathbf{f}_{ij} + \sum_W \mathbf{f}_{iW}. \quad (3)$$

The position vector $\mathbf{r}_i(t)$ is updated by the velocity $\mathbf{v}_i(t) = d\mathbf{r}_i/dt$.

The interaction force \mathbf{f}_{ij} between pedestrian i and j is specified as follows. With the distance $d_{ij} = \|\mathbf{r}_i - \mathbf{r}_j\|$ between the two pedestrians’ centres of mass, the psychological tendency of pedestrian i to stay away from pedestrian j is described by a repulsive interaction force $A_i \exp[(r_{ij} - d_{ij})/B_i] \mathbf{n}_{ij}$, where A_i and B_i are constants, indicating the strength and the range of the interaction, and $\mathbf{n}_{ij} = (n_{ij}^1, n_{ij}^2) = (\mathbf{r}_i - \mathbf{r}_j)/d_{ij}$ is the normalised directional vector pointing from pedestrian j to i . The pedestrians touch each other if their distance d_{ij} is smaller than the sum $r_{ij} = r_i + r_j$ of their radius r_i and r_j . In our model, we specify a uniform value for the size of each pedestrian (see Table I) [12]. While in reality the size of human body among the crowd is not uniform, previous work on 2D crystallisation shows that the size-polydispersity effect must be strong enough to disrupt the crystalline order [38]. The factor of size polydispersity among adult pedestrians is thus ignored in this work. Inspired by granular interactions, two additional forces are included in the model, which are essential for understanding the particular effects in panicking crowds: a “body force” $k(r_{ij} - d_{ij}) \mathbf{n}_{ij}$ counteracting body compression and a “sliding friction force” $\kappa(r_{ij} - d_{ij}) \Delta v_{ji}^t \mathbf{t}_{ij}$ impeding relative tangential motion, if pedestrians i and j are close enough. Here $\mathbf{t}_{ij} = (-n_{ij}^2, n_{ij}^1)$ means the tangential direction and $\Delta v_{ji}^t = (\mathbf{v}_j - \mathbf{v}_i) \cdot \mathbf{t}_{ij}$ the tangential velocity difference, while k and κ are large constants, representing the bump and the friction effect. In summary, the interaction force \mathbf{f}_{ij} between pedestrians i and j is given by

$$\mathbf{f}_{ij} = \{A_i \exp[(r_{ij} - d_{ij})/B_i] + kg(r_{ij} - d_{ij})\} \mathbf{n}_{ij} + \kappa g(r_{ij} - d_{ij}) \Delta v_{ji}^t \mathbf{t}_{ij}, \quad (4)$$

where the indicator function $g(r_{ij} - d_{ij})$ is zero for $r_{ij} - d_{ij} < 0$ and it is equal to $r_{ij} - d_{ij}$ otherwise.

The interaction with the walls is treated analogously. By denoting d_{iW} as the distance to wall W , \mathbf{n}_{iW} as the

direction perpendicular to it, and \mathbf{t}_{iW} as the direction tangential to it, we have

$$\mathbf{f}_{iW} = \{A_i \exp[(r_i - d_{iW})/B_i] + kg(r_i - d_{iW})\} \mathbf{n}_{iW} - \kappa g(r_i - d_{iW}) (\mathbf{v}_i \cdot \mathbf{t}_{iW}) \mathbf{t}_{iW}. \quad (5)$$

In the implementation of the SFM for large-scale systems, the most time-consuming part is to compute the interaction forces. For a N -particle system, the maximum number of pairwise interactions is $N(N-1)/2$, which leads to $O(N^2)$ time complexity. In this work we adopt the cell-list method [41] to avoid repeated calculation of pairwise interactions and thus significantly reduce the time complexity from $O(N^2)$ to $O(N)$ [42]. The cell-list method achieves this goal by dividing the physical space of the system into equal grids called cells. Each particle is assigned to a specific cell. In a two-dimensional system, each cell has eight neighbouring cells and a cell together with its eight neighbouring cells are called a cell neighbourhood (see Fig. 1). For each particle, we only need to calculate the interacting forces between the particles within the cell neighbourhood.

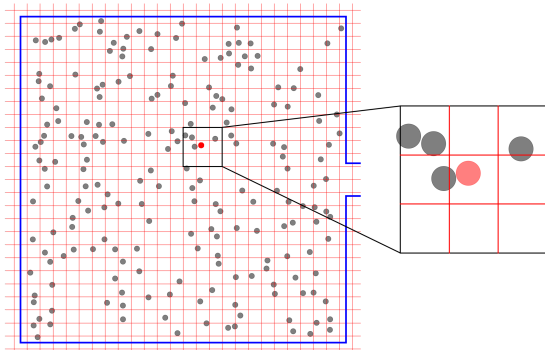


FIG. 1: Schematic plot of the simulation scenario. Pedestrians are depicted by dots and walls are depicted by blue lines with an open door in the right wall. Red grids are introduced to implement the cell-list method for efficiently computing the interaction forces. See the main text for more information.

III. RESULTS AND DISCUSSION

In this work we use the SFM to study a typical scenario of collective escape towards a single exit (see Fig. 1). Initially, N pedestrians are randomly distributed in a square room of side length H_0 , and the parameter values used in our simulation are presented in Table I, which largely follow Ref.12. For simplicity, the values for m_i , v_i^p , τ_i , r_i , A_i and B_i for each pedestrian are taken to be identical. The moment when the crowd start to run towards the exit is denoted as $t = 0$. In our simulation, the state of motion is updated according to eqn (3) by the time step Δt . In particular, the interaction forces between pedestrians are computed by the cell-list method. The edge

length of each cell is set to be $2r + 5B$ to ensure that the contribution from the next nearest neighbouring cells is negligibly small. The escape time for individual pedestrians is denoted as T_{es} , and the evacuation time for all the pedestrians to leave the room is denoted as T_{ev} .

TABLE I: List of parameters.

Variable	Value	Description
H_0	30 m	side length of the room
N	1000	number of pedestrians
m	80 kg	mass of pedestrians
v^p	1.0 m/s	desired velocity
τ	0.5 s	acceleration time
r	0.3 m	radius of pedestrians
A	2×10^3 N	interaction strength
B	0.08 m	interaction range
k	1.2×10^5 kg/s ²	bump effect
κ	2.4×10^5 kg/(m · s)	friction effect
Δt	0.001 s	time step in simulation

A. Collective escape statistics

We analyze several statistics regarding escape of the pedestrians. First, the simulations allow us to track the instantaneous collective escape rate, which is defined as the percentage of the pedestrians who have successfully exited the room: N_{out}/N where N_{out} is the number of escaped pedestrians. The rate N_{out}/N is plotted against time t in Fig. 2(a). The black curve is the average instantaneous escape rate over 6000 independent simulations with random initial conditions, and the red dashed curves show the results of several randomly selected sample simulation trials. From the figure, we see that, despite of the highly nonlinear behaviors of individual pedestrians, the collective escape rate exhibits a rather linear dependence on time over a long duration, indicating a steady outflow of pedestrians. The escape curve becomes saturated only at the end of the escape event, and the plateau lasts for a relatively short duration. The evacuation time T_{ev} of independent simulations is also analyzed statistically, and the results are shown in Fig. 2(b). The histogram of T_{ev} is approximately a normal distribution. The curve of the collective escape rate N_{out}/N and the histogram of the evacuation time T_{ev} imply the existence of statistical regularities underlying the highly complicated individual motions of pedestrians.

B. Formation of multiple fast tracks

In this section we further explore the escape dynamics of the crowd by examining the motion of individual pedestrians. In particular we are interested in this question: *Where are the relatively safer spots in the collective running of the pedestrians towards the exit?* To address this question, we focus on a group of pedestrians within

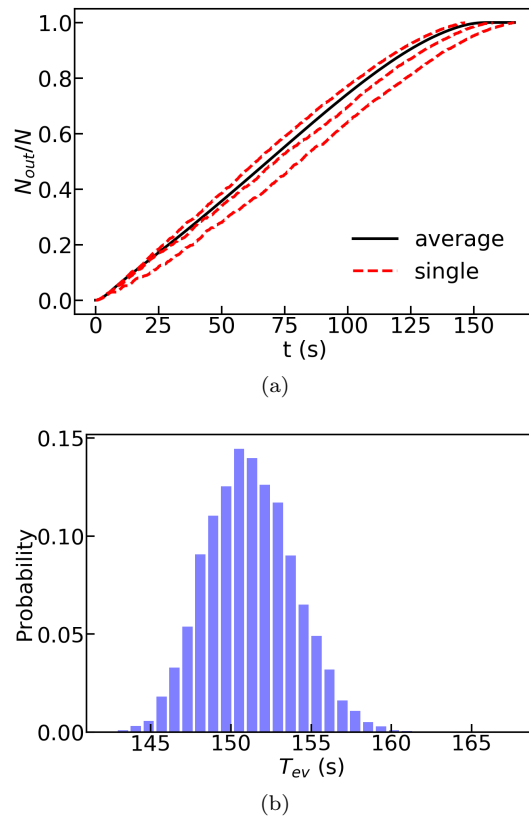


FIG. 2: Statistical analysis of the instantaneous escape rate in a typical scenario of collective escape towards a single exit. The escape rate is defined as the ratio N_{out}/N , where N_{out} is the number of pedestrians leaving the room. (a) Plot of N_{out}/N versus time. The black solid curve is the average instantaneous escape rate over 6000 independent simulations with random initial conditions. The escape rates of randomly picked simulation runs are also plotted in red dashed curves. (b) The distribution of the evacuation time T_{ev} for the 6000 simulations.

a narrow annulus around the exit, and track the escape time of these pedestrians. The selected pedestrians are indicated by red dots, as shown in Fig. 3. The distance between these pedestrians and the exit is approximately equal. In simulations, the annulus is created by drawing two adjacent circles centered at the door with the radii R_1 and R_2 , respectively. The annulus is then equally divided into a number of zones. The spanning angle of each zone is specified to ensure that each zone is occupied by pedestrians. We perform abundant independent simulations with random initial conditions.

By statistical analysis of the escape time of these pedestrians, we identify the safe spots where pedestrians spend the least time to escape. The lower panel in Fig. 3(a) shows anisotropic feature in the escape of crowd. The average escape time strongly depends on the angle ϕ , which is defined in the upper panel in Fig. 3(a). Remarkably, $\langle T_{es} \rangle$ reaches a deep minimum at $\phi = 90^\circ$. The average escape time of the pedestrians near $\phi = 90^\circ$

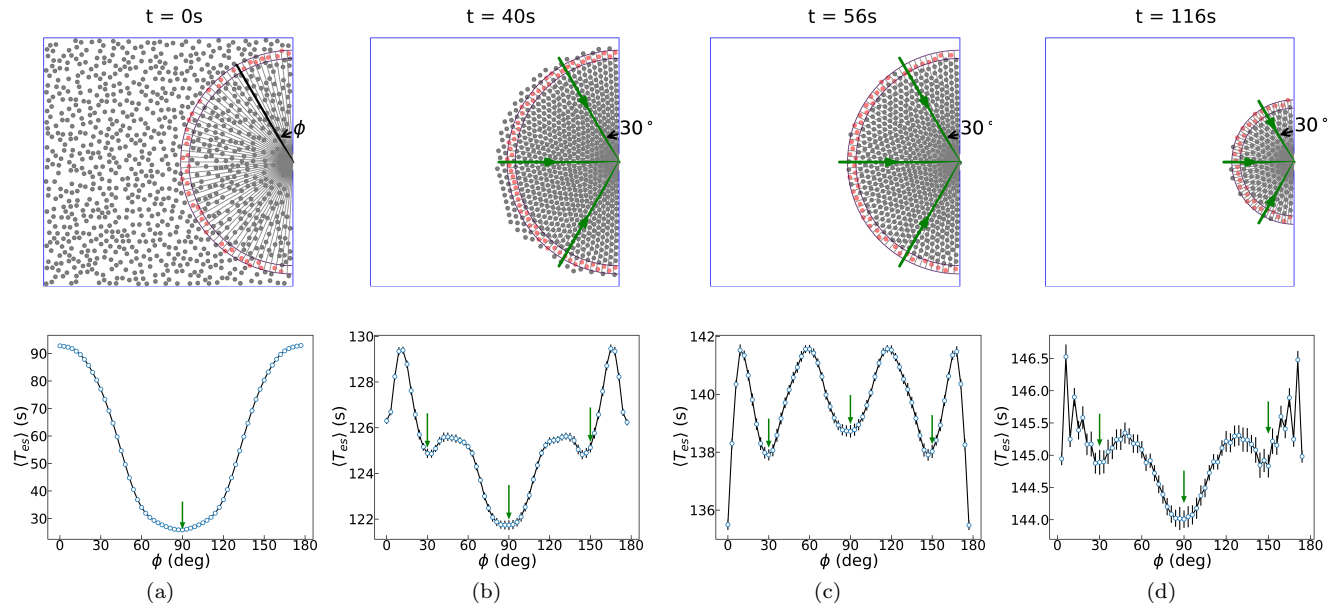


FIG. 3: Emergence of multiple fast tracks resulting from the spontaneously formed crystal structure in the escaping crowd. Typical snapshots of crowd configuration in the escape process are presented in the upper figures. The average escape time $\langle T_{es} \rangle$ of the pedestrians within the annulus between $R_1 = 13.5\text{m}$ and $R_2 = 12.5\text{m}$ (indicated by red dots) is shown in the corresponding lower figures; the smaller annulus in (d) is between $R_1 = 7.5\text{m}$ and $R_2 = 6.5\text{m}$; the averaging procedure is over 2000 independent simulations with random initial conditions and the error bars are obtained from 50 independent values of $\langle T_{es}(\phi) \rangle$. ϕ indicates the location of the pedestrian in the annulus. As the crowd is crystallised to a triangular lattice, valley structures emerge in the $\langle T_{es}(\phi) \rangle$ curve, which are identified as the fast tracks.

is only about a fourth of those near the wall. Therefore, the pedestrians who are initially along the axis perpendicular to the door spend significantly less time to escape than those near the wall. Note that analysis of the empirical data of individual crowd escape events also shows the anisotropy feature in the distributions of escape time, density and velocity in typical room evacuations [21, 43].

With the continuous outflow of the pedestrians, the crowd spontaneously form a compact circular configuration, as shown in Fig. 3(b)- 3(d). Note that no clogging occurs at the exit in our system due to the relatively low desired speed ($v^p = 1.0\text{ m/s}$); clogging may occur at high speed ($v^p > 1.5\text{ m/s}$) [12]. The local minima developed on the $\langle T_{es} \rangle$ - ϕ curves in Fig. 3(b) - 3(d) correspond to the relatively safe spots. Remarkably, with the outflow of the pedestrians, the trajectories of these safe spots constitute three straight lines along the specific angles of $\phi = 30^\circ$, 90° and 150° , as indicated by the green lines in the upper panels in Fig. 3. These lines are recognized as the fast tracks in the collective escape of the crowd.

Here, it is natural to ask if the anisotropic feature of escape time originates from the ϕ -dependent trajectories of pedestrians. To check this point, we examine the dependence of $\langle L \rangle / L_0$ on the angle ϕ . $\langle L \rangle$ is the mean actual length of the trajectory over independent simulation runs, and L_0 is the length of the straight line connecting the initial and final positions of a pedestrian at a specific angle ϕ . The actual trajectories of the pedestrians at $\phi = 15^\circ$ and $\phi = 90^\circ$ are indicated by the green

and red curves in Fig. 5(a). The plot of $\langle L \rangle / L_0$ versus the angle ϕ is presented in Fig. 5(b). From the $\langle L \rangle / L_0$ curves, which correspond to the four cases in Fig. 3, we see that the local minima do not match the angles of the fast tracks. As such, the emergence of the optimal angles could not be understood by the trajectory-based analysis. We are therefore led to examine the system from a new perspective.

C. The perspective of crystallisation and topological defects

The special angles of the fast tracks revealed in the preceding section provide an important clue. The appearance of these discrete fast tracks may be related to a global order developed in the compact packing of pedestrians.

To reveal the positional order of the pedestrians, we treat each pedestrian as a point and perform Delaunay triangulation of instantaneous crowd configuration by establishing bonds between each pedestrian and the nearest neighbours [37, 40]. This technique has been widely used to quantitatively analyze crystalline structures [37, 40]. An example of Delaunay triangulation is shown in Fig. 5(a). We see the regular arrangement of pedestrians in the form of a 2D triangular lattice; each vertex represents a pedestrian. Such a triangular lattice is disturbed by defects as indicated by colored dots.

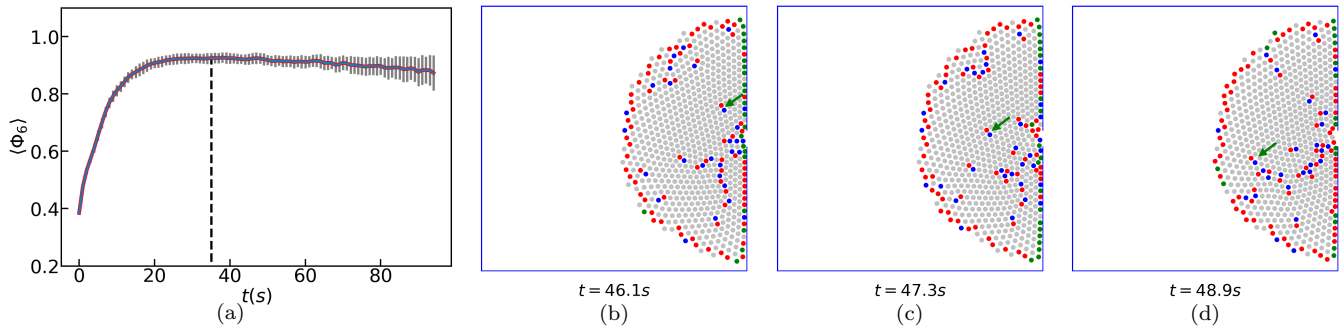


FIG. 4: Crystallisation process in the collective escape. (a) Temporal variation of the six-fold bond-orientational order parameter $\langle \Phi_6 \rangle$. The error bars are obtained from 100 independent simulations. The vertical dashed line indicates the time when the three fast tracks appear. (b)-(d) Glide motion of the dislocation as indicated by the green arrow in consecutive instantaneous configurations. The red and blue dots represent five- and seven-fold disclinations, respectively. A dislocation consists of a pair of five- and seven-fold disclinations.

Specifically, the red and blue dots represent pedestrians for whom the number of nearest neighbours (i.e., the coordination number) deviates from six. Note that in a perfect triangular lattice, the coordination number for each vertex is always six. These coloured dots therefore indicate the local disruption of the crystalline order. They are known as topological defects, since they cannot be eliminated by continuous deformation of the medium [37, 40]. A vertex with coordination number 5 and 7 are named five- and seven-fold disclinations, respectively. These disclinations are elementary topological defects in crystal lattice.

Interestingly, like electric charges, the disclinations carry topological charge that reflects their intrinsic property. Specifically, the topological charge of an n -fold disclination is $q = (6 - n)\pi/3$. Charge q is positive if $n < 6$ and negative if $n > 6$. According to elasticity theory, topological charges of the same sign repel and unlike signs attract, which is analogous to electric charges [38, 40]. The five-fold (red dots) and seven-fold (blue dots) disclinations tend to form pairs known as dislocations, as shown in Figs. 4(b)-4(d).

In connection with our system, the complicated process of achieving crystalline order in the compact crowd could be clarified by the concept of topological defects. With the outflow of pedestrians, the microscopic crystalline structure underlying the crowd is under persistent transformation. Simulations show that this dynamical process exactly corresponds to the characteristic annihilation and glide motion of topological defects in the crystal. Annihilation of positive and negative topological charges reduces the number of defects and leads to ordered arrangement of pedestrians. Furthermore, dislocations are abundantly generated near the exit with the outflow of pedestrians, and they tend to glide swiftly towards the boundary of the crowd. These two processes are crucial for achieving the crystallised state out of the initially highly disordered configuration [38, 39]. In Figs. 4(b) - 4(d), we show that the dislocation as indicated by the green arrow swiftly glides along the direction

that is perpendicular to the line connecting the five- and seven-fold disclinations [40]. In this typical scenario of glide motion, it takes about 2.7 seconds for the dislocation to move from the position at Fig. 4(b) to that at Fig. 4(d). In contrast, it takes about 8.4 seconds for a pedestrian of typical speed of 1m/s to cover the same distance.

The crystallisation process could be characterized by the six-fold bond-orientational order parameter [37]

$$\Phi_6 = \frac{1}{N} \sum_{i=1}^N \left| \frac{1}{n_b} \sum_{j=1}^{n_b} \exp(i6\theta_{ij}) \right|, \quad (6)$$

where n_b is the coordination number of the particle i , θ_{ij} is the angle between the line connecting the particles i and j and some chosen reference line, and N is the total number of particles. Note that, to characterize the interior crystalline order, a few layers of particles near the boundary and the exit are excluded in the calculation for the order parameter. The temporal variation of $\langle \Phi_6 \rangle$ is presented in Fig. 4(a); the error bars are obtained by statistical analysis of 100 independent simulations. The vertical dashed line indicates the time when the three fast tracks appear. This observation indicates the strong connection of the emergence of the three fast tracks and the full development of the crystalline order.

In the crystallised configuration of pedestrians, the principal axes of crystal are invariant regardless of the microscopic motions of topological defects. In fact, the transformation of the global crystalline structure which could modify the orientations of the principal crystallographic axes, requires the appearance of isolated disclinations; this is a highly energetically costly process [38]. In simulations, we observe that the orientations of the fast tracks are always along the three specific directions in the entire evacuation process. The central fast track that is perpendicular to the wall emerges even before the crystalline order is developed, as shown in Fig. 3(a). And in general it does not correspond to the principal axes of the crystal. The other two fast tracks make an angle of

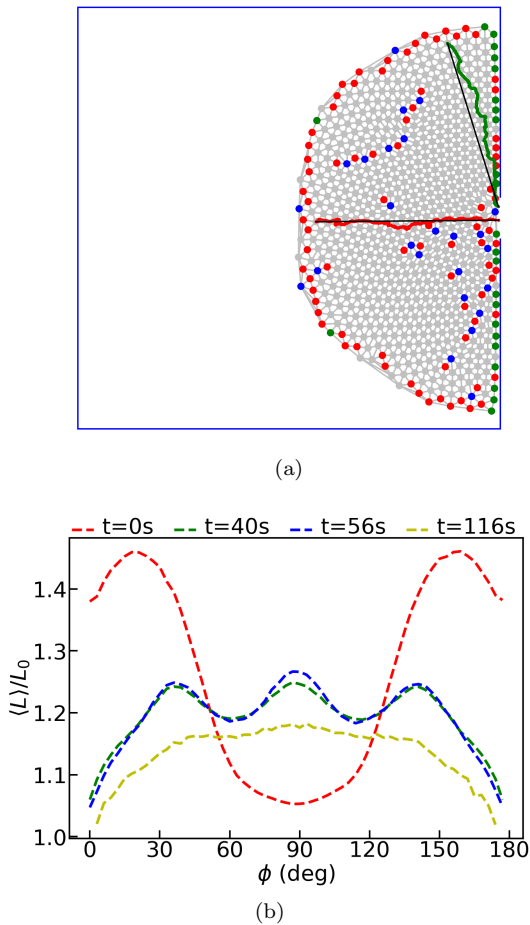


FIG. 5: Statistical analysis of single pedestrian trajectories. (a) Trajectories of typical pedestrians (see the red and green curves) in the crystallised crowd. Crystallographic defects are indicated by coloured dots. See the main text for more information. (b) Plot of $\langle L \rangle / L_0$ versus the angle ϕ . $\langle L \rangle$ is the mean actual length of the trajectory over 2000 independent simulations with random initial conditions, and L_0 is the length of the straight line connecting the initial and final positions of a pedestrian at a specific angle ϕ .

$\pi/3$ with respect to the central one; this specific angle is a signature of the triangular lattice. The stability of the global crystalline order well explains the invariance of the orientations of the fast tracks. To conclude, the formation of the fast tracks in the collective escape of human crowds has strong connection with the global crystalline order developed in the configuration of pedestrians.

D. Effects of uncertainty in human behaviours

As mentioned earlier, the motion of pedestrians is unambiguously determined by the physical and socio-psychological forces. However, the behaviours of pedestrians in a crowded environment could exhibit some degree of uncertainty as affected by fluctuating psycholog-

ical state and rapidly varying local environment. We model the uncertainties in human behaviour by incorporating a random force into the model. Here, we emphasize that adding a noise term to the original deterministic SFM also provides an opportunity to test the robustness of the model. The generalized social force model is

$$m_i \frac{d\mathbf{v}_i}{dt} = m_i \frac{v_i^p(t) \mathbf{e}_i^p(t) - \mathbf{v}_i(t)}{\tau_i} + \sum_{j(\neq i)} \mathbf{f}_{ij} + \sum_W \mathbf{f}_{iW} + \mathbf{f}_i^N, \quad (7)$$

in which the noise term \mathbf{f}_i^N is given by

$$\mathbf{f}_i^N = c \frac{mv^p}{\tau} \epsilon_i. \quad (8)$$

The white noise ϵ_i follows a two-dimensional Gaussian distribution $N(\mathbf{0}, \mathbf{I}_2)$. This approach takes into account the flexible usage of space by pedestrians, which is essential to reproduce the empirical observations in a natural and robust way [2]. The prefactor c in eqn (8) reflects the relative strength of the noise force in comparison with the personal desire force. Note that eqn (7) represents a particular active Brownian dynamics [44]. The active force originates from the tendency for each pedestrian to move towards the exit, and the noise term is for modelling the uncertainties in human behaviour. While the values of the parameters in the model are specified according to Ref.12 by comparison with experiments, the variation of these parameters implies the richness in the collective dynamics of the active agents. The investigation of eqn (7) as a model of active Brownian dynamics in the parameter space is beyond the scope of this work.

To systematically investigate the effect of the random behaviour of pedestrians, we vary the strength of the noise by tuning the value of c in eqn.(8). Crystallisation phenomenon is observed uniformly as the value of c is increased from 0.1 up to 100. The plot of $\langle T_{es} \rangle$ versus ϕ under varying c is presented in Fig. 6(a). For reference, the noise-free case of $c = 0$ is also plotted. Figure 6(a) shows that adding a modest noise force does not qualitatively alter the behaviours of the system, suggesting the robustness of the model. When the value of c is as large as 100, the crowd exhibits global migration which obscures the concept of fast tracks. We also notice that the collision of the crowd with the wall leads to a density wave propagating through the entire system. See Supplemental Materials for the videos of the simulated crowd dynamics at $c = 0$, $c = 10$, and $c = 100$ using the parameters in Table I.

E. Dilemma of escape strategy

We proceed to discuss the scenario of collective escape if all the pedestrians know and adopt the strategy of running towards the *central fast track*. To address this issue, we add a tendency force on each pedestrian towards the

line of the central fast track, and update the crowd configuration by

$$m_i \frac{d\mathbf{v}_i}{dt} = m_i \frac{v_i^p(t) \mathbf{e}_i^p(t) - \mathbf{v}_i(t)}{\tau_i} + \sum_{j(\neq i)} \mathbf{f}_{ij} + \sum_W \mathbf{f}_{iW} + \mathbf{f}_i^T. \quad (9)$$

For simplicity, \mathbf{f}_i^T is designed to be the gradient of a quadratic potential $U_i = \frac{1}{2} b d_i^2$, where d_i is the vertical distance from the pedestrian i to the central horizontal line. The tendency force increases linearly with d_i . b is the controlling parameter for the strength of the tendency force. By writing b in the form of $b = 2c' m v^p / H_0 \tau$, the relative strength of the tendency force is controlled by c' . The plot of $\langle T_{es} \rangle$ vs ϕ is presented in Fig. 6(b). Increasing c' leads to the elevation of the curves. It indicates that when all the pedestrians adopt the escape strategy, the average evacuation time increases. Nevertheless, the relatively safe spots are still located along the central line; the relative advantage of the central line is reduced.

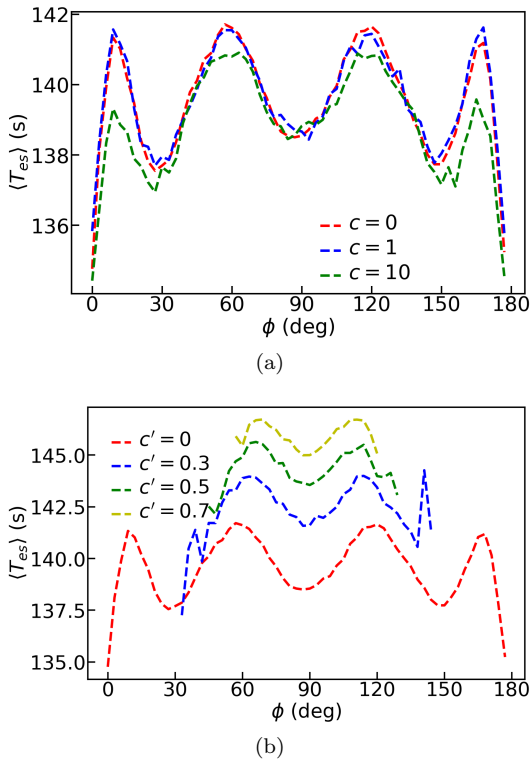


FIG. 6: Plot of the average escape time $\langle T_{es} \rangle$ of the pedestrians within the annulus over 2000 independent simulations with random initial positions at varying conditions. The record of the escape time starts at $t = 56$ s for comparison with Fig. 3(c). (a) Increasing the uncertainty in decision-making, as modelled by the noise level in the model, does not affect the basic valley structures in the $\langle T_{es}(\phi) \rangle$ curve. (b) Including the tendency of pedestrians towards the central fast track boosts the global risk. See the main text for more information.

Finally, we emphasize that the results presented in this work are derived from the theoretical SFM without considering relevant factors in reality, such as the situation of injury and the intelligent adaption of pedestrians to local environment. And we emphasize that the results derived in this work that is based on the SFM are subject to experimental examination. Here, we briefly discuss the social force model itself. This model has proven a powerful tool to simulate complicated crowd dynamics by incorporating the socio-psychological element into the force model. However, the socio-psychological forces in the model can be disputable. It is natural to inquire to what extent the subtle psychology and action of pedestrians upon various external stimuli can be characterised by these forces. Our simulations suggest that the emergent statistical law underlying the crowd dynamics is unaffected by the modest random variation of individual behaviour. This observation provides good evidence on the reliability of the statistical laws derived from the model. But under larger fluctuations of individual behaviours, such as non-local migration of pedestrians, one has to revise the forces. A direction of interest is to design smart rules of motion that endow the particles with more free will; the spirit of combining the physical and socio-psychological elements may be retained in the new model [45].

IV. CONCLUSION

In summary, by conducting symmetric simulations with the social force model, we have revealed the ordering driven multiple fast tracks in collective escape of human crowds, and clarified the underlying mechanism by the exploiting the striking analogy of crowd dynamics and crystallisation. Notably, the emergent topological defects and their characteristic dynamics play a crucial role for shaping the global crystalline order and creating the fast tracks. It is important to emphasize that, it is not our intention to advocate any specific model of crowd dynamics. Although our analysis in this work is based on the simulation results of SFM, we conjecture, however, that the analysis methods proposed as well as the link between crowd dynamics and crystallisation are not dependent on SFM. To this end, it is of interest to explore such a link using other popular crowd dynamics models [46, 47] and further validate our analysis. Moreover, we appreciate that the proposed mechanism interpretation needs to be further validated by experimental studies, and we believe that such mechanism may provide useful information towards more efficient crowd evacuation management.

V. ACKNOWLEDGMENTS

This work was supported by NSFC Grants No. 16Z103010253.

- [1] D. Helbing and P. Molnar, *Phys. Rev. E* **51**, 4282 (1995).
- [2] D. Helbing, L. Buzna, A. Johansson, and T. Werner, *Transp. Sci.* **39**, 1 (2005).
- [3] D. Helbing, A. Johansson, and H. Z. Al-Abideen, *Phys. Rev. E* **75**, 046109 (2007).
- [4] N. Gravish, G. Gold, A. Zangwill, M. A. Goodisman, and D. I. Goldman, *Soft matter* **11**, 6552 (2015).
- [5] Y. Z. Tao and L. Y. Dong, *Europhys. Lett.* **119**, 10003 (2017).
- [6] C. Rogsch, M. Schreckenberg, E. Tribble, W. Klingsch, and T. Kretz, in *Pedestrian and evacuation dynamics 2008* (Springer Berlin Heidelberg, 2010), pp. 743–755.
- [7] J. Adrian, M. Amos, M. Baratchi, M. Beermann, N. Bode, M. Boltes, A. Corbetta, G. Dezecache, J. Drury, Z. Fu, et al., *Collective Dynamics* **4**, 1 (2019).
- [8] L. Gibelli and N. Bellomo, *Crowd Dynamics, Volume 1: Theory, Models, and Safety Problems* (Springer, 2019).
- [9] A. Rahouti, R. Lovreglio, P. Jackson, and S. Datousaid, in *Proceedings of the 9th International Conference on Pedestrian and Evacuation Dynamics (PED2018)* (2018).
- [10] C. Feliciani and K. Nishinari, in *Proceedings of the 9th International Conference on Pedestrian and Evacuation Dynamics (PED2018)* (2018).
- [11] R. A. Smith and J. F. Dickie, *Engineering for crowd safety: proceedings of the International Conference on Engineering for Crowd Safety* (Elsevier Science Ltd, 1993).
- [12] D. Helbing, I. Farkas, and T. Vicsek, *Nature* **407**, 487 (2000).
- [13] M. Batty, J. DeSyllas, and E. Duxbury, *Int. J. Geogr. Inf. Sci.* **17**, 673 (2003).
- [14] T. Metivet, L. Pastorello, and P. Peyla, *Europhys. Lett.* **121**, 54003 (2018).
- [15] M. Moussaïd, N. Perozo, S. Garnier, D. Helbing, and G. Theraulaz, *PloS one* **5**, e10047 (2010).
- [16] J. James, *Am. Sociol. Rev.* **18**, 569 (1953).
- [17] D. J. Sumpter, *Philos. Trans. R. Soc. B-Biol. Sci.* **361**, 5 (2006).
- [18] C. Castellano, S. Fortunato, and V. Loreto, *Rev. Mod. Phys.* **81**, 591 (2009).
- [19] A. Schadschneider, W. Klingsch, H. Klüpfel, T. Kretz, C. Rogsch, and A. Seyfried, *Evacuation Dynamics: Empirical Results, Modeling and Applications* (Springer, New York, NY, 2009), pp. 3142–3176, 1st ed.
- [20] T. I. Lakoba, D. J. Kaup, and N. M. Finkelstein, *Simulation* **81**, 339 (2005).
- [21] I. Zuriguel, I. Echeverria, D. Maza, R. C. Hidalgo, C. Martín-Gómez, and A. Garcimartín, *Saf. Sci.* **121**, 394 (2020).
- [22] M. Chraïbi, T. Ezaki, A. Tordeux, K. Nishinari, A. Schadschneider, and A. Seyfried, *Phys. Rev. E* **92**, 042809 (2015).
- [23] M. Boltes, J. Zhang, A. Tordeux, A. Schadschneider, and A. Seyfried, *Empirical Results of Pedestrian and Evacuation Dynamics* (Springer, Berlin, Heidelberg, 2018), pp. 1–29, 2nd ed.
- [24] J. Cordes, A. Schadschneider, and A. Tordeux, arXiv preprint arXiv:1911.07547 (2019).
- [25] D. Helbing and A. Johansson, *Pedestrian, Crowd and Evacuation Dynamics* (Springer, New York, NY, 2009), pp. 6476–6495, 1st ed.
- [26] L. Henderson, *Nature* **229**, 381 (1971).
- [27] L. F. Henderson, *Transportation Research* **8**, 509 (1974).
- [28] D. Helbing, *Complex Systems* **6**, 391 (1998).
- [29] D. Bauer, S. Seer, and N. Brändle, in *Proceedings of the 2007 summer computer simulation conference* (Society for Computer Simulation International, San Diego, CA, USA, 2007), pp. 1035–1042.
- [30] D. Helbing, M. Isobe, T. Nagatani, and K. Takimoto, *Phys. Rev. E* **67**, 067101 (2003).
- [31] A. Cziráok and T. Vicsek, *Physica A* **281**, 17 (2012).
- [32] M. Chraïbi, A. Tordeux, A. Schadschneider, and A. Seyfried, *Modelling of Pedestrian and Evacuation Dynamics* (Springer, Berlin, Heidelberg, 2018), pp. 1–22, 2nd ed.
- [33] A. Corbetta, J. A. Meeusen, C.-m. Lee, R. Benzi, and F. Toschi, *Phys. Rev. E* **98**, 062310 (2018).
- [34] M. Das, C. F. Schmidt, and M. Murrell, *Soft Matter* **16**, 7185 (2020).
- [35] D. Helbing, *Behavioral Sci.* **36**, 298 (1991).
- [36] A. Colombi and M. Scianna, *R. Soc. Open Sci.* **4**, 160561 (2017).
- [37] D. R. Nelson, *Defects and geometry in condensed matter physics* (Cambridge University Press, Cambridge, UK, 2002).
- [38] Z. Yao and M. Olvera de la Cruz, *Proc. Natl. Acad. Sci. USA* **111**, 5094 (2014).
- [39] Z. Yao, *Soft Matter* **12**, 7020 (2016).
- [40] P. Chaikin and T. Lubensky, *Principles of condensed matter physics* (Cambridge University Press, Cambridge, UK, 2000).
- [41] M. Matin, P. Daivis, and B. Todd, *Comput. Phys. Commun.* **151**, 35 (2003).
- [42] M. Dobson, I. Fox, and A. Saracino, *J. Comput. Phys.* **315**, 211 (2016).
- [43] A. Garcimartín, J. M. Pastor, C. Martín-Gómez, D. Parisi, and I. Zuriguel, *Scientific Reports* **7**, 1 (2017).
- [44] F. Schweitzer and J. Farmer, *Brownian Agents and Active Particles* (Springer, 2007).
- [45] F. Martínez-Gil, M. Lozano, and F. Fernández, in *International Workshop on Adaptive and Learning Agents* (Springer, Berlin, Heidelberg, 2011), pp. 54–69.
- [46] P. Fiorini and Z. Shiller, *The International Journal of Robotics Research* **17**, 760 (1998).
- [47] B. Ulicny and D. Thalmann, in *Computer Graphics Forum* (Wiley Online Library, 2002), vol. 21, pp. 767–775.